Influence of Chamber Geometry and Operating Conditions on the Performance of Feedback-Free Fluidic Oscillators

Eric J. Meier and Stephen D. Heister
Purdue University, West Lafayette, IN, 47907, USA, ejmeier@purdue.edu

ABSTRACT
The feedback free fluidic oscillator uses the unsteady nature of two colliding jets to create a single oscillating outlet jet with a wide sweep angle. These devices have the potential to provide additional combustion control, boundary layer control, thrust vectoring, and industrial flow deflection. The work presented in this paper uses two-dimensional computational fluid dynamics, CFD, to analyze the jet oscillation frequency over a range of operating conditions and to determine the effect that geometric changes in the oscillator design have on the frequency. In addition, microphone data gathered from six 3D printed fluidic oscillators is used to validate the CFD and correlate the 2D analysis to several different oscillator aspect ratios. Results presented in this paper illustrate the changes in jet oscillation frequency with gas type, gas temperature, operating pressure, pressure ratio across the oscillator, aspect ratio of the oscillator, and the frequency trends with various changes to the oscillator geometry.

1. INTRODUCTION

A fluidic oscillator, a type of flow control actuator, is a device with no moving parts which creates an unsteady oscillating outlet jet solely due to the internal fluid dynamics. These devices work with a variety of fluids from liquids to gases, and with a range of jet oscillation frequencies from a few Hertz to over 25 kHz with jet sweep ranges up to +/– 60 degrees as determined by past experimental and computational studies [1–8].

With accurate design, fluidic oscillators can be integrated into rocket and gas turbine injector elements with the goal of enhancing combustion control. Acoustic speakers or high-speed valves may be used to impose oscillations, but these systems have substantially greater complexity than active fluidic devices. Valves are typically limited to a few hundred Hz making them insufficient for applications demanding kilo-Hertz pulsations. For example, speaker and valve approaches have been utilized in both gas turbine and rocket combustors with open loop control configurations resulting in a significant reduction in combustion instability at certain modulation frequencies [9–16]. Similar instability control can be achieved through the use of fluidic oscillators as their oscillation frequency provides steady propellant modulation in open loop control without the need for speakers and high speed valves. A previous experiment saw up to a 40% reduction in combustion instability pressure oscillations when modulating the fuel flow with a fluidic oscillator in a bluff body combustor [17]. In addition, the oscillating jet action of the fluidic oscillator can be used to enhance mixing thereby increasing combustion control. Fluidic oscillators offer a step forward in combustion control due to their high reliability as they require no electrical power or actuating parts to operate. Further applications for fluidic oscillators include boundary layer control over aircraft wings [18–20], thrust vectoring and industrial flow deflection [21], and jet noise reduction [22].

Fluidic oscillators are divided into two main categories, the feedback fluidic oscillator and the feedback free fluidic oscillator. The feedback oscillator uses the Coanda wall attachment effect with designs that date back to 1962 [23]. These designs normally consist of a single inlet jet with two feedback loops [24]. Feedback oscillators can create one sweeping jet or multiple binary pulsing outlet jets, also called flip-flop nozzles, depending on their design [25]. The feedback free oscillator first developed by Raghu in 2001, uses two inlet jets impinging in an interaction chamber to create a single sweeping outlet jet [26].

1.1. Feedback Free Fluidic Oscillator

The basic design of the feedback free fluidic oscillator is illustrated in Fig. 1. As labeled in Fig. 1, the oscillator consists of two supply fluid jets, S1 and S2, impinging in the interaction chamber, IC, where the fluids are mixed and expelled out the exit, EX, as a single oscillating jet, SJ. The two impinging supply jets, S1 and S2, create an unstable stagnation point which causes them to oscillate within the interaction chamber. This phenomena was first witnessed by Denshchikov during submersed experiments with head on impinging water jets [27]. While the origin of the impinging jet oscillations is understood, the effects of different fluid types, flow rate conditions, and geometric configurations have complicated the study and characterization of feedback free fluidic oscillators.

Following the development of the feedback free fluidic oscillator in 2001, numerous studies both computational and experimental have looked to further understand the oscillation mechanism within the enclosure and the design factors that determine the oscillation frequency and jet sweep angle. Gregory et al. used pressure sensitive paint to experimentally visualize the two pairs of counter rotating vortices formed within the interaction chamber and to measure the amount of mixing between two gaseous fluids [3]. Tomac et al. further enhanced experimental visualization of the internal flow dynamics through particle image velocimetry, PIV, measurements using sodium iodide as the working fluid [4, 28, 29]. Bidadi et al. compared frequencies between liquid and gaseous fluid operation and found that air operating at the same pressure had oscillation frequencies almost twenty times higher than water [1]. Both Tomac and Bidadi performed computational fluid dynamics, CFD, on their experimental designs and found the internal fluid dynamics closely matched their experimental observations [1, 4, 5]. Bidadi's experimental frequency measurements with water closely matched the frequencies from his two-dimensional, 2-D, CFD, however, experimental measurements for air were not performed [1]. Tomac found that his three-dimensional, 3-D, CFD model agreed with his experimental results for air within 3% while his 2-D CFD results were up to 50% lower than the experimental measurements [5]. These results showed that the third dimension of depth of the oscillator can be important in the analysis of gaseous oscillator operation.

Using his experimental data, Gregory developed a non-dimensional scaling parameter to describe the frequency for the oscillators based on geometric dimensions and volumetric flow rates that agreed within 50% error [4, 30]. Gregory's scaling parameter uses the oscillation frequency, volumetric flow rate, and dimensions of the oscillator throat. Later, Tomac, working with Gregory, greatly improved the accuracy of the scaling parameter by taking into account the root mean square, rms, averaged location of the saddle point in the interaction chamber as determined from PIV measurements [5]. The corrected scaling factor was able to predict frequencies in the low, transitional, and high flow rate regimes. Unfortunately, this corrected scaling factor requires knowledge from experimental PIV measurements and cannot be used to evaluate new, un-tested designs.

This work presents a visualization of the oscillation cycle with high flow rate compressible gases along with a more comprehensive description for the effect of operating conditions on the jet

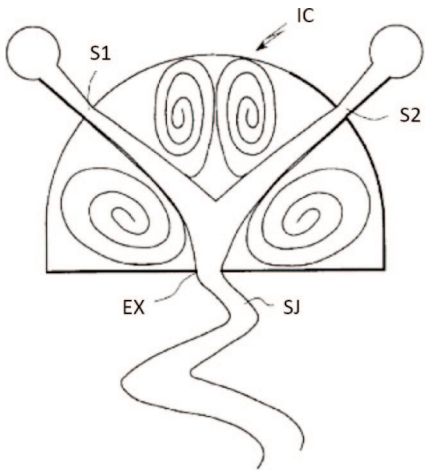

Figure 1. The feedback free fluidic oscillator oscillation cycle is controlled by the two pairs of counter rotation vorticies formed within the interaction chamber. The merging of the co-rotating vortex pairs drives the outlet jet in a controlled, oscillatory manner [26].

oscillation frequency. This study evaluates effects such as gas type, inlet temperature, overall operating pressure, and pressure ratio across the oscillators. In addition, a correction factor to match the 2-D CFD analysis to experimental conditions for various oscillator depths is presented. This allows the 2-D CFD to account for inherent 3-D effects caused by the oscillator depth or thickness as noted by Tomac and Gregory [4]. The effect of various geometric changes including size scaling, supply jet injection angle, and interaction chamber modifications on the jet oscillation frequency are also investigated. These results will serve as guidelines for designers to adjust the oscillator design to meet specific frequency ranges at their operating conditions. Data gathered in this study influenced the design of a fluidic oscillator for rocket combustion instability suppression.

2. COMPUTATIONAL MODEL DEVELOPMENT

The CFD analysis utilized 2-D unsteady compressible flow with a second order pressure coupled solver which solves the momentum and pressure-based continuity equations. The platform for the 2-D unsteady analysis was the ANSYS® FLUENT® 14.5.7 CFD package [31]. The model uses constant pressure inlets and a constant pressure outlet along with no-slip wall boundary conditions. Surface monitors at the inlets, throat, along the width of the outlet-box, and vertically along the outlet-box were used to capture the oscillation frequency and flow rate conditions as shown in Figure 2. Constant pressure boundary conditions were selected for their relevance to flow control applications. Due to the high exit Reynolds number, the turbulent k-ω SST model was employed. A simulated outlet-plenum at the oscillator exit was incorporated into the model in order to visualize and measure the outlet jet oscillation sweep angle. A structured mesh size of 53,000 elements accurately predicted the results when compared to finer meshes for the baseline case as shown in Table 1. Using the baseline mesh density, a parametric study was conducted to assess the influence of geometric designs, operating temperatures, operating pressures, and different operating gases. The last 37 ms of data gathered at 1 MHz provided a frequency resolution of 27 Hz. The time step used in the CFD analysis was 1 μs. The last 37 ms of data was processed in MATLAB using a Fast Fourier Transform, FFT, analysis to calculate the jet oscillation frequencies.

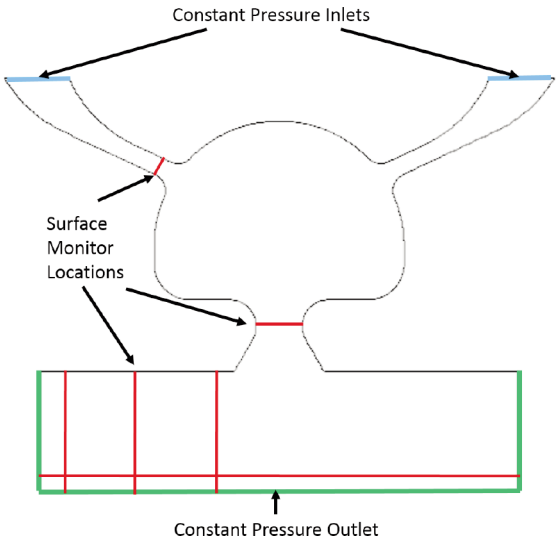

Figure 2. Illustration showing CFD model boundary conditions and monitor locations.

Table 1. Results from mesh convergence Study

Mesh	Elements	Jet Frequency (Hz)	Mass Flow Rate (g/s)
Coarse 0.5x	12960	1250	1.045
Coarse 0.75x	30650	1450	0.992
Baseline	52956	1430	0.995
Refine 1.25x	86117	1430	0.997
Refine 1.75x	169876	1430	0.996

Figure 3 illustrates the fluidic oscillator designs considered for the geometric study. The baseline design is similar in terms of supply jets and chamber design to the fluidic oscillators studied by Gregory and Tomac [2–4, 28, 29]. The supply jet design remained constant for all designs considered. The throat design eliminated the manufacturing difficulties encountered with the sharp edges used by Bidadi et. al. [1] Designs 02 through 06 adjusted the interaction chamber area and flow path for the upper and lower vortex pairs. Designs 07 and 08 explored the jet impingement height within the interaction chamber. Supply jet width was investigated in Designs 09 and 10 while Design 11 enlarged the supply jet and the throat. Designs 12 and 13 adjusted the throat width while Design 14 kept the throat width the same, but expanded the outlet nozzle angle.

Figure 4 shows several geometric parameters extracted from these designs based on their effect on the jet impingement location, vortex formation, and residence time in the interaction chamber. The corresponding dimensions as designed for each oscillator are given in Table 2. The parameter L1 describes the distance from the injection point to the jet impingement point in the center of the interaction chamber, L2 is the horizontal distance between the two jet impingement points, W_i is the width of the supply jet, H1 and H2 are the upper and lower chamber half heights, W_t is the throat width, and α is the inlet jet injection angle. Note that the internal jet impingement point was determined by the intersection of straight lines from the center of the supply jets at the jet injection angle. The upper chamber half height, H1, is the vertical distance from the impingement point to the maximum chamber height. This value was implemented to better capture the distance the oscillating jets move in Designs 04 through 06.

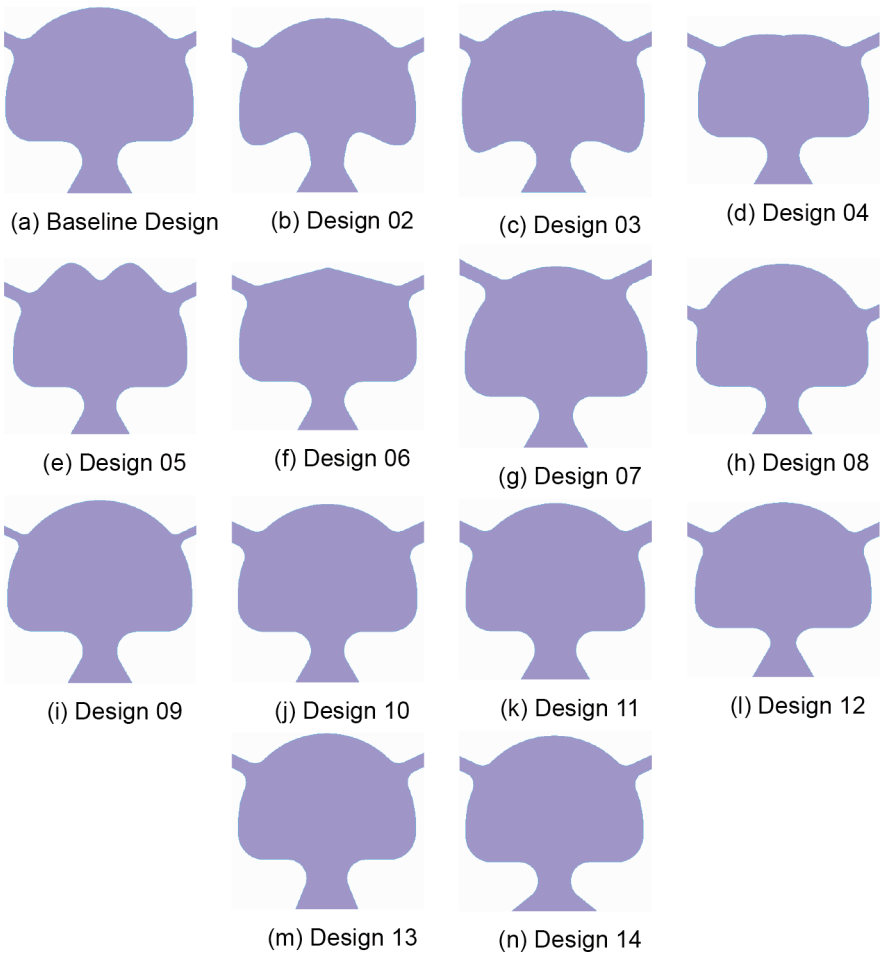

Figure 3. Fluidic oscillator designs considered for geometric characterization. The designs focused on adjusting the volumetric flow rate through the inlet and outlet width adjustments and the vortex sizes through the inlet injection angles, injection height, and the interaction chamber design.

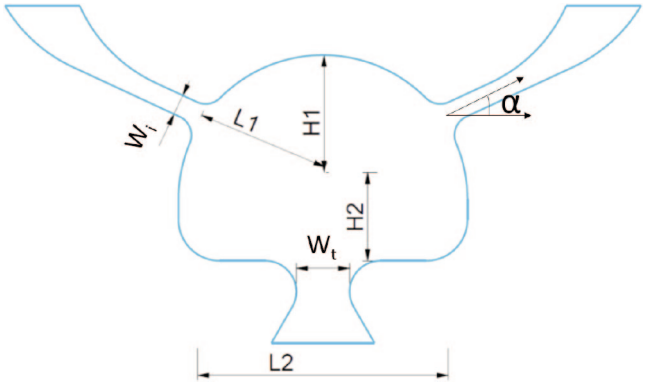

Figure 4. Feedback free fluidic oscillator with driving dimensions as determined by the CFD geometry study.

Table 2. Oscillator design geometry data. All dimensions in mm except for area (mm^2)

Model	Chamber Area	L1	L2	W_i	H1	W_t	H2	α
Baseline	271	9.5	17.3	1.5	8.5	3.9	6.6	25°
D-02	270	9.5	17.3	1.5	8.5	3.9	6.6	25°
D-03	291	9.5	17.3	1.5	8.5	3.9	6.6	25°
D-04	247	9.5	17.3	1.5	6.2	3.9	6.6	25°
D-05	273	9.5	17.3	1.5	8.5	3.9	6.6	25°
D-06	252	9.5	17.3	1.5	7.0	3.9	6.6	25°
D-07	271	7.2	13.0	1.5	5.3	3.9	9.7	25°
D-08	271	11.3	19.6	1.5	11.3	3.9	3.7	25°
D-09	271	9.5	17.3	0.9	8.5	3.9	6.6	25°
D-10	271	9.5	17.3	2.3	8.5	3.9	6.6	25°
D-11	271	9.5	17.3	2.3	8.5	4.8	6.6	25°
D-12	271	9.5	17.3	1.5	8.5	3.0	6.6	25°
D-13	271	9.5	17.3	1.5	8.5	4.8	6.6	25°
D-14	271	9.5	17.3	1.5	8.5	3.9	6.6	25°
Printed Design	152	7.9	15.8	1.1	7.9	2.9	3.4	35°

3. EXPERIMENTAL SETUP

While the 2-D CFD allowed for an in-depth characterization, it neglected the effects of the oscillator's third dimension of depth or thickness. To augment the 2-D CFD analysis, experiments were performed using a baseline oscillator design manufactured six times at different oscillator depths with nitrogen gas as the working fluid. The depth is considered the distance into the page in Figure 4 and is illustrated in Figure 6b. The experimental setup employed sonic venturis with sizes ranging from 0.229 mm to 0.711 mm in diameter in order to limit the nitrogen mass flow rates thereby allowing for more precise control over the fluidic oscillator supply pressures. The venturis were integrated upstream of a common manifold that fed both oscillator inlets. The fluidic oscillator test articles consisted of a 1/4" inlet feeding a common manifold which feed both oscillator inlets as seen in Figure 5a. A 1/8" pressure transducer port on the back side of the manifold allowed for measuring of the oscillator supply pressure as seen in Figure 5b. The test articles were constructed using the PolyJet 3-D printing process with the FullCure 720 transparent material on a Stratasys Objet Eden 350 printer. This process was selected due to its high accuracy and the ease of removal of the internal support material. The PolyJet printer allows for layer thicknesses as small as 0.016 mm resulting in build tolerances of +/–0.13 mm.

The design of the printed fluidic oscillator resulted from the CFD analysis with a targeted oscillation frequency above 3000 Hz with nitrogen gas due to future rocket applications in the frequency range. The resulting design is similar to a reduced size baseline design with an overall interaction chamber width of 15.8 mm, interaction chamber height of 11.3 mm, inlet width of 1.1 mm, and throat width of 2.9 mm. The size reduction was necessary to increase the oscillation frequency to the desired 3000 Hz range.

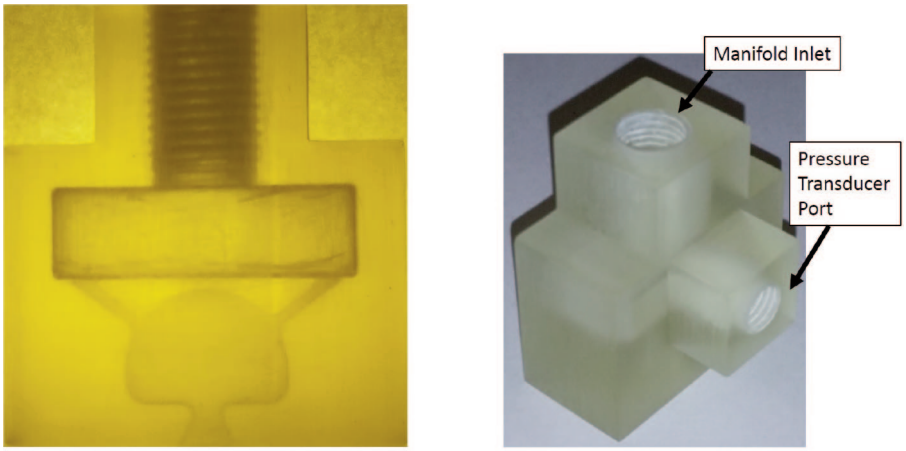

(a) Front view (b) Isometric view

Figure 5. The 3-D printed fluidic oscillator design used for experimental testing included a common manifold with a pressure transducer port to mimic the constant pressure boundary conditions in the CFD analysis.

Table 3. Printed oscillator measured dimensions. All dimensions in mm

Oscillator Design	Depth Designed/Printed	Throat Width Designed/Printed	Aspect Ratio Error	Cd*A (mm^2)
Printed 01	1.0/1.02	2.9/2.71	8.13%	1.2
Printed 02	1.5/1.49	2.9/2.87	0.68%	2.0
Printed 03	2.0/2.07	2.9/2.83	5.62%	2.4
Printed 04	2.5/2.46	2.9/2.81	1.71%	3.4
Printed 05	2.9/2.91	2.9/2.83	2.68%	3.1
Printed 06	3.5/3.57	2.9/2.78	5.97%	3.9

The as printed dimensions for the throat width and depth are shown in Table 3 along with the percent error from the designed aspect ratio. Also shown in Table 3 are the flow discharge coefficient values, Cd, based on the measured throat area in mm^2. It should be noted that the low aspect ratio cases of test articles, Printed 05 and 06, have the lowest Cd values of the designs printed. This could suggest additional viscous losses present in the low aspect ratio designs although additional testing is required to confirm this. Based on the measured throat dimensions, similar errors are expected for the internal dimensions. The throat and depth dimensions were measured using a Hirox KH-8700 3-D digital microscope with a few example images looking down into the oscillator throat shown in Figure 6. The microscope was focused on the throat region as indicated in Figure 6b allowing the image to look past the outlet width on the oscillator base. The printer was able to accurately match the design depth although it resulted in a smaller throat width for each of the printed oscillators. The printer error grew near the sharp corners giving the throat rounded corners when it should ideally be a rectangle. The parts also resulted at a slight angle when looking down into the oscillator as evident by the blurry shading on the inside of the throat on the left side in Figure 6a. While the angle of the built part does not affect the 2-D oscillation nature, the consistency of the build angle could not be confirmed due to the limitations of the microscope optics. The focus length of the digital microscope was insufficient to accurately measure the internal dimensions of the fluidic oscillators.

The manifold pressures were measured at 1 Hz using a Druck PMP 1260 pressure transducer with a range of 0 to 413 kPa with a 1–5 Vdc output. A microphone placed near the jet exit as shown in Figure 7, captured the high frequency acoustic measurements from the jet oscillations. The microphone data was gathered at 20 kHz for 10 seconds from a PCB Piezotronics microphone, model 378B02, through a National Instruments dynamic signal acquisition board, PCI-4472. Experimental results were read into MATLAB and compared with the CFD oscillation frequency results to determine a correction factor for the depth that minimized the absolute error for each test article.

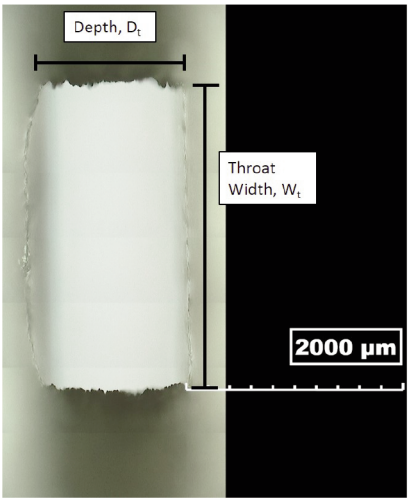

(a) Printed Design 02 (Aspect Ratio = 1.93)

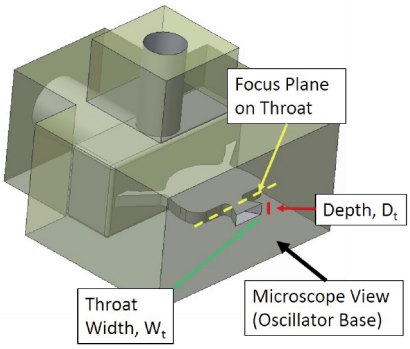

(b) Oscillator and microscope view orientation.

Figure 6. Digital microscope images were used to measure throat width and depth of the 3D printed fluidic oscillators. Note that the black in the images indicates the edge of the microscope imaging, not the edge of the oscillator base.

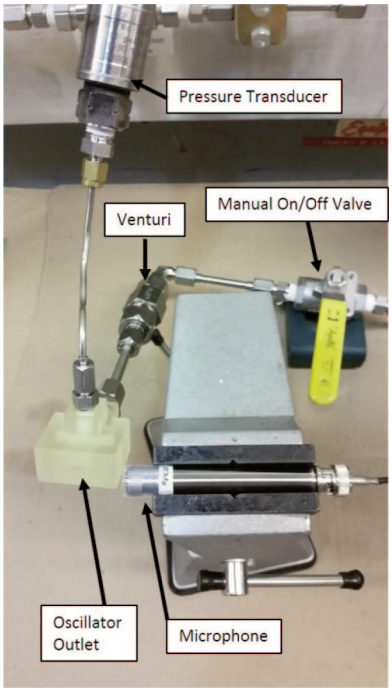

Figure 7. The experimental setup placed a microphone near the fluidic oscillator outlet in order to accurately capture the jet oscillation frequency.

4. RESULTS

The CFD analysis provides for high fidelity visualization of the vortex interactions within the interaction chamber during the oscillation cycle. Analysis with the baseline oscillator design focused on assessing the jet oscillation frequency changes with operating gas type, inlet temperature, operating pressure, and pressure differential across the oscillators. An oscillator depth study focused on experiments to support the 2-D CFD trends and also to assess frequency changes with increasing oscillator depths. An investigation of geometric changes to the interaction chamber, supply jets, and outlet nozzle focused on determining key geometric dimensions and their effect on frequency.

Except for the different pressure ratios and overall pressure cases, all CFD cases were run with a 135.62 kPa inlet boundary condition and 101.325 kPa outlet boundary. Except for the temperature variation cases, all inlet and outlet temperatures were kept at 300 K with gaseous nitrogen as the working fluid. A summary of the CFD analysis cases completed for each investigation is shown in Table 4. A large number of cases were required to capture the jet oscillation frequency dependence on the inlet to outlet pressure ratio for the geometric designs.

4.1. Jet Oscillation Phenomena At High Flow Rates

The CFD results for high flow rate nitrogen gas illustrate the unstable nature of the vortex interactions within the baseline chamber design. Figure 8 shows velocity magnitude colored streamlines for one complete oscillation cycle of the baseline oscillator design with a jet oscillation frequency of 1,430 Hz. The cycle is dominated by the formation of two counter-rotating vortex pairs in the upper and lower portions of the chamber. During the cycle, vortex merging of the co-rotating vortices within the interaction chamber causes the supply jets to move within the chamber, thus driving the outlet jet oscillations as seen in Figures 8d and 8e. The merging of one pair of co-rotating vortices creates a single large vortex that dominates the interaction chamber as shown in Figure 8d. This large vortex pushes the opposite supply jet away from the outlet, giving the supply jet feeding the large vortex complete control of the outlet. The supply jet that is cut off from the outlet begins feeding its much smaller lower vortex. Feeding the smaller vortex allows it to grow in strength while the large vortex is weakened due to its supply jet flowing through the outlet as shown in Figure 8e. Eventually the lower left vortex gains enough strength to merge with its co-rotating vortex as shown in Figure 8f which starts the next cycle.

Smaller vortices from the supply jet shear layer are formed at various points in the cycle in addition to the two counter-rotating vortex pairs as seen in Figures 8a, 8b, and 8f. This happens several times during the cycle where the smaller, co-rotating shear layer vorticies merge to form the large vortex structures that drive the jets. Previously observed liquid jets saw the formation of two counter rotating vortex pairs with the merging of one pair during the cycle [1, 4, 5, 28]. The higher flow rates give the impinging jets enough energy to completely cut each other off from the outlet jet during the cycle. This phenomena has also been seen by Tomac in PIV images of high flow rate liquids through fluidic oscillators [5].

In addition to the outlet jet oscillation, the mass flow rate of the jet oscillates at twice the outlet jet frequency. During the oscillation cycle, the maximum mass flow rate occurs when each jet has control of the outlet while the minimum occurs when the jets are competing for the outlet control. The throat mass flow rate time history and outlet jet sweep angle for the baseline oscillator at a pressure ratio of 1.34 are illustrated below in Figures 9a and 9b. Since the analysis was 2-D, the mass flow rate in ANSYS® FLUENT® is extrapolated based on a 1 m deep oscillator. This output was scaled based on a 1.5 mm oscillator depth to give estimated flow rates for experiments and integration of similarly sized oscillators. Figure 9b shows average jet sweep angles of +/– 60 degrees for the baseline design.

4.2. Gas Type and Inlet Temperature

The operating gas type for the Baseline design varied across a range of gases from hydrogen to benzene giving an inlet density range from 0.1 kg/m^3 to 3.6 kg/m^3. The changes in gas type resulted in large frequency changes due to the variation in volumetric flow rate caused by the gas density differences.

Table 4. Summary of total CFD analysis cases completed

CFD Analysis Investigations	Total CFD Analysis Cases Completed
Geometry Supply Jet Angle	45
Geometry Interaction Chamber	71
Geometry Supply and Outlet Sizing	48
Baseline Design Size Scaling	64
Inlet to Outlet Pressure Ratio	35
Overall Operating Pressure	20
Inlet Gas Temperature	8
Working Fluid Gas Density	13
Depth Characterization	43

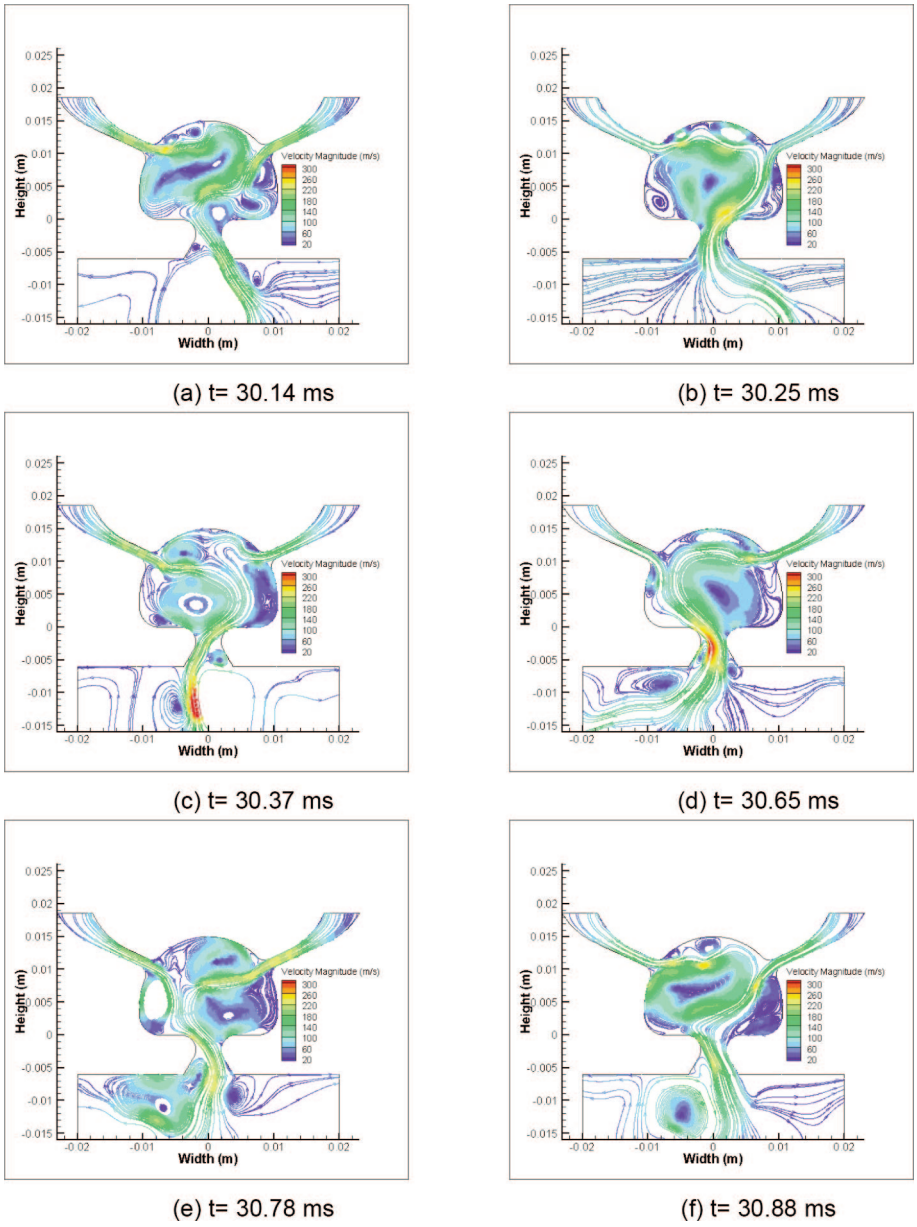

Figure 8. Velocity magnitude streamtrace illustration of one oscillation cycle shows vortex merging between the co-rotating vortex pairs that drives the outlet jet oscillation.

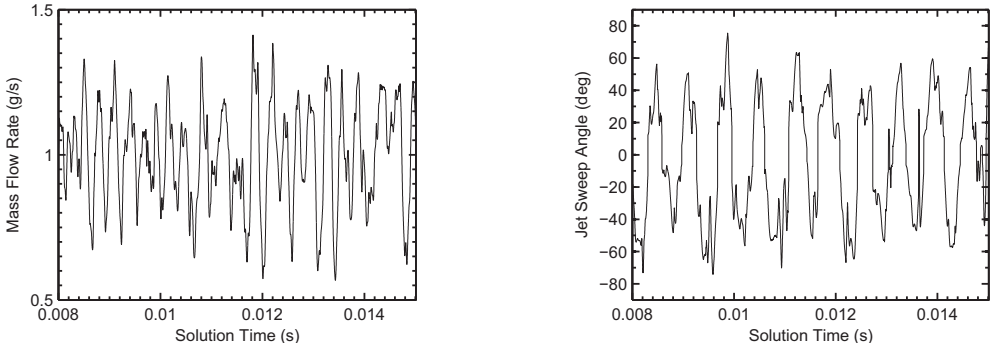

(a) Mass flow rate oscillation at the oscillator throat. (b) Outlet jet sweep angle from 2-D CFD.

Figure 9. Data gathered during 2-D CFD illustrates the oscillatory nature of the outlet jet and mass flow rate.

While the oscillation frequencies see an exponential increase with decreasing gas density, the frequency scales linearly with the volumetric flow rate through the oscillator. Analysis of the inlet temperature variation saw similar results due to the reduction in gas density and thus an increase in volumetric flow rate for the increasing inlet gas temperatures. The inlet gas temperatures varied from 300 K to 1500 K with nitrogen gas. Results illustrating these trends are shown in Figure 10 and in Table 5 . Previous studies that included data from the high volumetric flow rate regime, above 4×10^{-6} m^3/s, saw a similar linear frequency trend with increasing volumetric flow rate [2, 28].

4.3. Overall Operating Pressure

The overall operating pressure cases kept the inlet to outlet pressure ratio constant at 1.33 while increasing the overall pressure, the average of inlet and outlet pressures, from 120.66 kPa to 3.103 MPa. The pressure ratio is defined as p_i/p_s where P_i is the supply jet pressure and P_o is the pressure of the oscillator outlet environment. Figure 11 illustrates that the jet oscillation frequency is only minimally

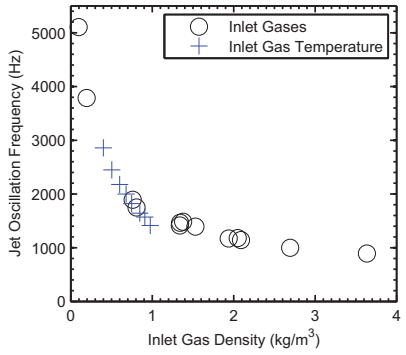

(a) The outlet jet oscillation frequency varied exponentially with inlet gas density.

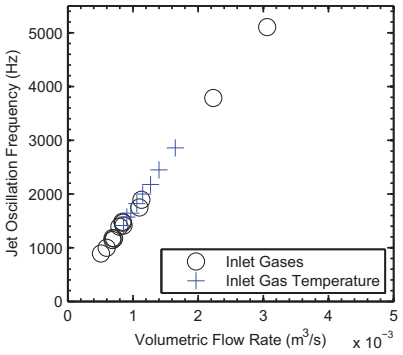

(b) The outlet jet oscillation frequency varied linearly with the oscillator volumetric flow rate.

Figure 10. The outlet jet frequency variation from the operating gas type and the inlet temperature analysis.

Table 5. Gas density and inlet temperature results sorted by inlet density for baseline design at pressure ratio = 1.34

Model	Inlet Density (kg/m^3)	Volumetric Flow Rate (m^3/s)	Jet Frequency (Hz)
Hydrogen	0.097	0.003	5100
Helium	0.195	0.002	3786
Inlet Temp 1500 K	0.266	0.0017	2860
Inlet Temp 1000 K	0.398	0.0014	2450
Inlet Temp 750 K	0.534	0.0013	2180
Inlet Temp 600 K	0.67	0.0012	2000
Methane	0.76	0.0011	1890
Inlet Temp 500 K	0.806	0.0011	1820
Ammonia	0.808	0.0011	1750
Inlet Temp 400 K	1.004	0.001	1640
Inlet Temp 350 K	1.151	0.0009	1570
Nitrogen	1.34	0.0009	1410
Carbon Monoxide	1.343	0.0009	1460
Air	1.38	0.0008	1480
Oxygen	1.53	0.0008	1390
Argon	1.94	0.0007	1170
Propane	2.05	0.0007	1180
Carbon Dioxide	2.09	0.0007	1140
Butane	2.693	0.0006	1000
Benzene	3.636	0.0005	890

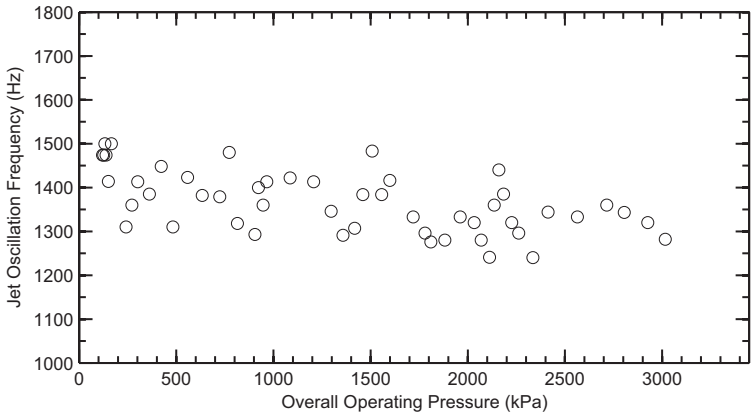

Figure 11. Overall operating pressure did not greatly effect on the outlet jet oscillation frequency when the overall pressure ratio was held constant.

effected by operating pressure as long as the relative inlet to outlet pressure ratio remains constant. Results showed that the jet oscillation frequency decays less than 10% over the operating pressure range considered. This trend allows designers to test oscillators in atmospheric conditions to determine the oscillation frequency they will see in high pressure combustor conditions at the same pressure ratio where measuring the frequency is more difficult. The grid density study results outlined in Table 1 suggests that the variation in Figure 11 is due to second order viscous interactions within the oscillator and not random variation within the CFD model.

4.4. Pressure Ratio

The pressure ratio, defined by the supply pressure divided by the outlet pressure was adjusted by keeping the outlet boundary at 101.325 kPa while increasing the inlet supply boundary pressure. As seen in Figure 12 a linear trend is seen up to a pressure ratio of 1.5 after which the frequency becomes asymptotic with pressure ratio. Eventually at higher pressure ratios around 2.25, the oscillator becomes fully choked, thereby limiting the volumetric flow rate increase at higher pressure ratios which prevents the oscillation frequency from increasing. The vertical lines on Figure 12 indicate the transition from linear to asymptotic and from asymptotic to fully choked. The higher pressure ratio of 2.25 for a choked condition compared to 1.89 for steady jets, results from additional viscous losses in the interaction chamber due to the jet interactions as well as losses in the narrow inlet channels.

4.5. Depth Correlation Results

Six different experiments with fluidic oscillators of various depths as noted in Table 3, agreed with the CFD frequency trend with pressure ratio and were also used to determine a depth correction factor to

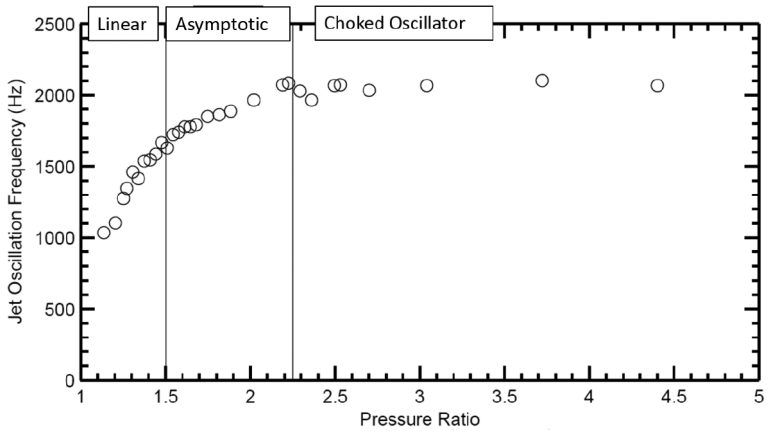

Figure 12. The outlet jet oscillation frequency increases with increasing pressure ratio until a pressure ratio of 2.25. Near this point, the oscillator becomes asymptotic and there is no additional frequency increase with increasing the pressure ratio beyond 2.25.

match the 2-D CFD with the experimental oscillators. Table 6 shows the oscillator aspect ratio, AR, as determined by $AR = w_t/D_t$ where W_t is the throat width and D_t is the oscillator depth. Also shown in Table 6 is the correction factor used to correct the 2-D CFD to match the frequencies of various aspect ratios and the coefficient of determination value, R^2, accompanying each correction factor. Experimental trends closely matched the CFD results as seen by the corrected results in Figure 13.

Table 6. Printed oscillator aspect ratio and CFD depth correction factor

Design	D_t (mm)	W_t (mm)	AR	CFD Correction Factor	R^2
Printed 01	1	2.9	2.90	1.39	0.950
Printed 02	1.5	2.9	1.93	1.32	0.990
Printed 03	2	2.9	1.45	1.26	0.984
Printed 04	2.5	2.9	1.16	1.17	0.978
Printed 05	2.9	2.9	1.00	1.41	0.986
Printed 06	3.5	2.9	0.83	1.56	0.158

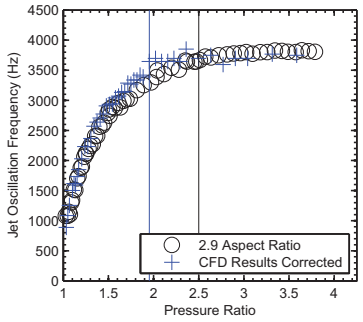

(a) Printed 01 oscillation frequency

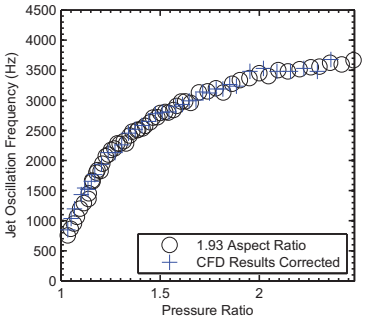

(b) Printed 02 oscillation frequency

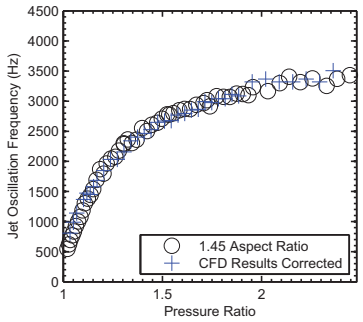

(c) Printed 03 oscillation frequency

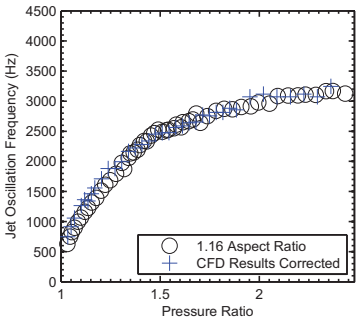

(d) Printed 04 oscillation frequency

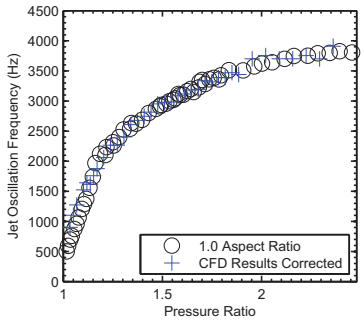

(e) Printed 05 oscillation frequency

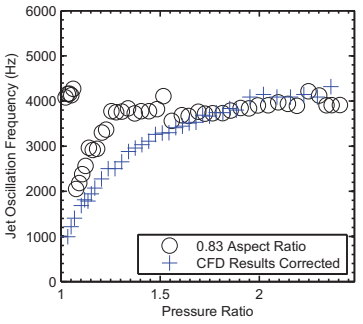

(f) Printed 06 oscillation frequency

Figure 13. The CFD jet oscillation frequency trend compared very well with the experimental results when the scalar correction factor to the CFD data was applied. For low aspect ratio cases (oscillator depth > outlet width), the flow is more three-dimensional resulting in a poor comparison with the two-dimensional CFD.

The CFD correction factor, CF, is a scalar multiple determined by $f_{actual} = CF * f_{CFD}$, that was used to correct the CFD frequency values to match the experimental results at each aspect ratio. Printed Design 06 with an aspect ratio of 0.83 was the only design that did not match the CFD trend as shown in Figure 13f and indicated by the low R^2 value in Table 6. This mismatch is due to the low aspect ratio which enables the flow to become more three-dimensional creating a large disconnect from the two-dimensional CFD calculations. A closer look at the data reveals harmonics indicating that Printed 06 is still oscillating despite the off-nominal behavior when compared to the high aspect ratios [32]. Previous experimental results at various oscillator depths with low flow rate air and water saw a reduction in oscillation frequency with a decrease in aspect ratio [4]. It should be noted that the correction factors are model specific, however, the results show the validity of the 2-D CFD models in capturing the oscillation mechanism for oscillator aspect ratios greater than 1.0.

A closer look at Printed Design 01, the high aspect ratio case, shown in Figure 13a illustrates the CFD transition to a choked oscillator condition occurs sooner than the experimental results show. The vertical lines illustrate the point of transition to a choked oscillator for the CFD and experimental results. This is due to the wall friction on the faces of the printed oscillators which works to limit the flow rate through the oscillators thereby postponing the transition to a choked oscillator condition where the frequency no longer increases with increasing pressure ratio. The two-dimensional CFD was unable to take the wall friction from the front and back faces of the oscillator into account.

4.6. Geometry Study Results

An attempt was made to correlate, using 2-D CFD, the effect of various geometric changes to the oscillator inlet, outlet, and interaction chamber to changes in the jet oscillation frequency. The goal was to determine the most critical oscillator dimensions and their effect; enhancing or reducing, on the jet oscillation frequency. The study consisted of 15 different geometric designs shown in Figure 3 along with five different supply jet injection angles and five linearly scaled variations of the baseline design.

4.6.1. Fluidic oscillator size scaling

The jet oscillation frequency scales consistently with the oscillator size scale factor at each operating pressure ratio as shown in Figure 14a. While the frequency varies over the nine operating conditions considered, the relative change in frequency for each of the scaled designs does not change significantly. The oscillation frequency scales with Eq. 1, where S_f is the scale factor, f_{scaled} is the frequency of the scaled design, and $f_{Baseline}$ is the frequency of the baseline design. The scale factor is determined by $S_f = Size/Baseline\ Size$ such that a 1/4 size oscillator will have a scale factor of 0.25 resulting in a four fold increase in oscillation frequency over the baseline size. All of the scaled designs followed the same trend with increasing pressure ratio as evident by Figure 14b where all of the oscillation frequencies collapse to the baseline value when multiplied by the scale factor. The 0.25 scaled design did not oscillate at the 1.13 pressure ratio condition. This could be due to the viscous effects in the smaller, 4.75 mm wide, interaction chamber in the 0.25 scale design dominating the fluid flow at the low pressure ratio.

$$f_{scaled} = f_{Baseline}/S_f \tag{1}$$

4.6.2. Fluidic oscillator supply and outlet design modifications

The effect of the supply jet injection angle on the oscillation frequency is minimal in the range of 5° to 40° as seen in Figure 15a. While the effect of the injection angle on the frequency changes with operating pressure ratio, the close grouping especially at higher pressure ratios suggest that the minimal effect is only seen at lower flow rates. These finding are similar to the CFD results from Bidadi et al. who analyzed fluidic oscillators with very high pressure ratios with air as the working fluid [1]. The 35 degree injection angle design did not oscillate at the 1.13 pressure ratio condition.

The supply and outlet design changes effect on frequency, shown in Figure 15b, scale closely with the volumetric flow rate through them. Design 09 with the smaller supply jets is consistently the lowest in frequency at lower flow rates. The smaller throat in Design 12 reduces the oscillation frequency especially at higher pressure ratios. The supply jet size effects the oscillation frequency at lower pressure ratios with the larger supply jets in Design 10 leading to higher frequencies when compared to the baseline case and Design 09 with smaller supply jets. At higher operating pressure ratios, the supply jet size does not effect the frequency and the oscillation becomes limited by the throat width.

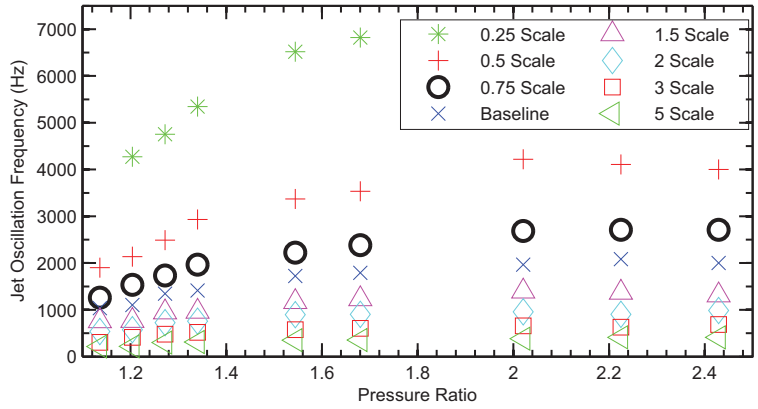

(a) The outlet jet oscillation frequency scaled linearly with the scale of the baseline fluidic oscillator design with smaller oscillators resulting in much higher oscillation frequencies.

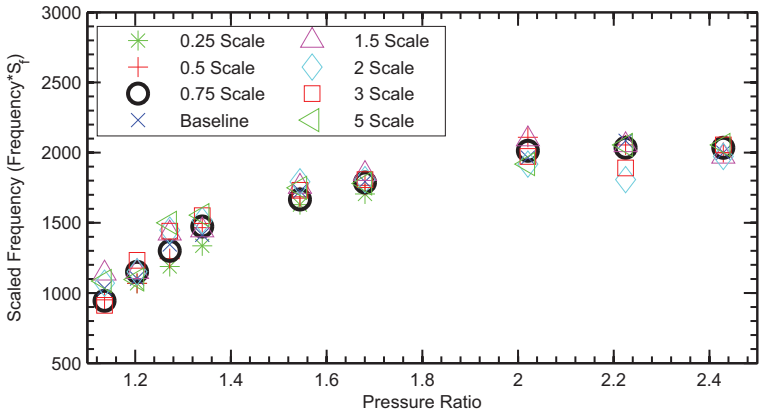

(b) The frequencies for the different sized oscillators collapse back to the baseline frequency when multiplied by the design size scale factor.

Figure 14. The oscillation frequency scales linearly with size and collapses back to the baseline frequency when multiplied by the scale factor over the entire range of pressure ratios considered.

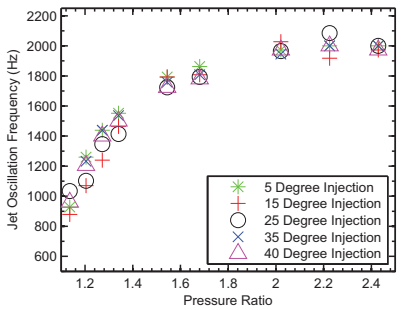

(a) The inlet injection angle did not seem to greatly affect the outlet jet oscillation frequency based on the CFD analysis.

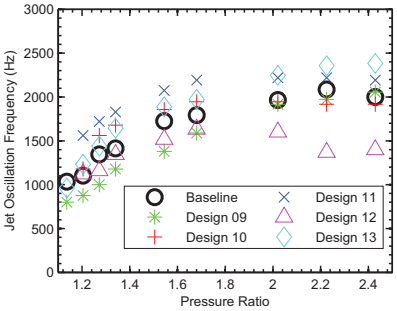

(b) The oscillator inlet and outlet design changes resulted in increased oscillation frequency for designs that increased the total volumetric flow rate.

Figure 15. Geometric inlet and outlet effects on the outlet jet oscillation frequency.

Design 11 with the larger supply jets and larger throat width allowed for a much higher total volumetric flow rate resulting in higher oscillation frequencies. Design 13 with the baseline supply jet size and larger throat saw an increase in oscillation frequency over the baseline case. This increase over the baseline grew as the operational pressure ratio increased.

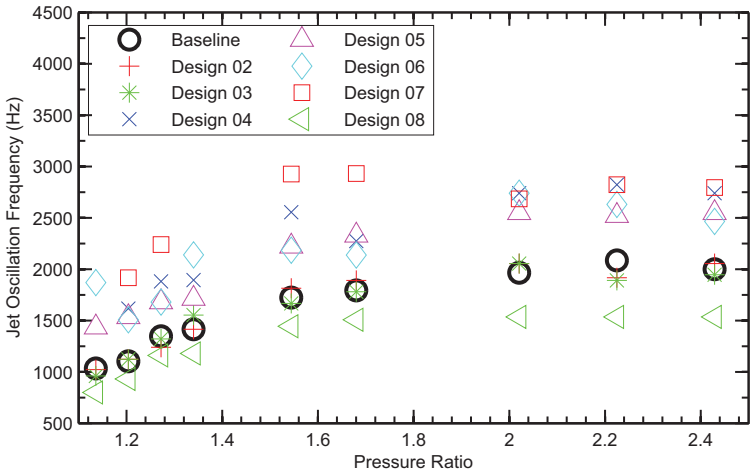

Figure 16. Interaction chamber designs resulting in smaller top chamber area and close proximity of the inlet jets resulted in higher jet oscillation frequencies. Modifications of the lower portion of the interaction chamber had no major effect on the jet frequency.

In general, the greater the volumetric flow rate capability of the supply jets and the outlet of a feedback free fluidic oscillator, the higher the frequency. In addition, Designs 10–12 did not oscillate at the 1.13 pressure ratio condition. Design 14 with the larger outlet nozzle width, had very little effect on the oscillation frequency and did not enhance the jet oscillation spray angle. This suggests that the width of the outlet nozzle is not a limiting factor and that the spray angle is determined by other geometric factors including the interaction chamber geometry and the throat design.

4.6.3. Fluidic oscillator interaction chamber design modifications

Figure 16 illustrates the effect of various interaction chamber design modifications on the jet oscillation frequency. Designs 02 and 03 are consistently near the baseline design which leads to the conclusion that the location and size of the lower vortices do not significantly drive the jet oscillations. Designs 04–07 vary in their relative effect on the oscillating frequency over the operating conditions, however, all three designs exhibited noticeable increases in frequency over the baseline design. Data for these six designs shows that the vortices in the top portion of the interaction chamber have a much greater effect on the oscillating frequency than the lower vorticies. Design 07 with the smallest H1 distance, has the highest oscillation frequency over the pressure ratio ranges considered. The smaller H1 distance reduces the distance the oscillating jets travel to reach the top of the interaction chamber and complete the cycle thereby reducing the oscillating time. In addition to the smaller H1 value, Design 07 also has the smallest distance between the inlet jets, L2 and L1. Design 08 with the lower supply jet injection height consistently had the lowest oscillation frequency over the range of operating conditions as it has the largest H1, L1, and L2 values. Prior studies looking at impinging jet mixing for reacting injection molding, RIM, have seen oscillations decrease with increasing head distance, H1, and also decrease with increasing distance between the jets, L1 as shown in Figure 4 [33, 34]. This explains the frequency change from Designs 07 and 08 with smaller head distance and closer proximity impinging jets resulting in higher frequencies. Since the jets are limited by the flow rate and the speed of sound at choked conditions, the increased distances lower the frequencies over all flow rates as seen with Design 08. Additional RIM studies found that jets with little or no head distance above the impinging jets had no recirculation zone in the top region which can have a stabilizing effect on the flow field [35]. This could help explain why Design 04 and 07 with their small H1 distance did not exhibit oscillations under certain low flow rate conditions. Design 04 did not oscillate at the 1.13 pressure ratio and Design 07 did not oscillate at the 1.13 and 1.34 pressure ratio conditions.

5. CONCLUSIONS

Two-dimensional CFD analysis was used to characterize the performance of the feedback free fluidic oscillator subject to changes in gas type, operating condition, and geometric changes to the oscillator itself. Gas type and the inlet gas temperature greatly affect the frequency of the oscillating outlet jet due

to the changes in gas density and volumetric flow rate through the oscillators. The oscillation frequency increases linearly with increasing volumetric flow rate resulting from decreasing inlet gas density. The CFD analysis also showed that the jet oscillation frequency only decays minimally for fixed pressure ratio operation as the overall operating pressure is increased up to a value of 3.1 MPa. This allows designers to test oscillators at atmospheric conditions and obtain similar oscillator performance as they would see in a much higher pressure environment with the same pressure ratio. Adjustment of the pressure ratio has a large effect on frequency from 1.1 to 1.5 with high pressure ratios leading to significantly higher frequencies. At pressure ratios higher than 1.5, frequencies asymptote to a value consistent with the oscillator choking condition.

An experimental study with the baseline oscillator at six different depths allowed for correlation of the 2-D CFD results to match oscillator frequencies at various aspect ratios. While the 2-D CFD requires a correction factor based on aspect ratio to predict oscillator frequencies, it does prove accurate for aspect ratios greater than 1. The 2-D CFD with 53,000 elements offers a substantial reduction in computation time compared to previous 3-D CFD models which required 1,500,000 elements [5]. The great reduction in computational time allows designers to quickly run models to assess oscillation frequencies at hard to test operating conditions such as high outlet pressures and assess performance with volatile fluids.

While a concise correlation of jet oscillation frequency to geometric parameters proved difficult due to the lack of consistency in the relative frequency change over various operating pressure ratios, several conclusions were made from the data. The jet oscillation frequency scales linearly with the scale factor over a variety of operating conditions. The supply jet injection angle has a minimal effect on the oscillation frequency at low pressure ratios, but that small effect diminishes at higher pressure ratios. The supply jet and outlet design effect the jet oscillation frequency by increasing or decreasing the available flow rate through the oscillators. In general, the higher the flow rate at a given pressure ratio, the higher the jet oscillation frequency although the frequency increase is limited by the resistance of the oscillator. At high pressure ratios, the oscillator becomes choked and frequency is limited by the throat width regardless of the supply jet size. While many of the changes to the interaction chamber varied in their effect on frequency over the range of operating conditions, changes to the lower portion of the chamber affecting the lower vortices has a minimal effect on frequency. Changes to the top portion of the chamber has significant effects on increasing the frequency suggesting the top vortices have a more dominant effect on the jet oscillations. The height of the supply jet injections caused changes to the upper chamber height, H1 and the distance between the jets, L1 and L2. Decreasing H1, L1, and L2 causes a reduction in the distance the oscillating jets travel to reach the top of the chamber, thereby increasing the jet oscillation frequency. Increasing these distances has the reverse effect and decreases the frequency. Similar observations have been made in studies of impinging jets in reaction injection molding systems [33, 34].

ACKNOWLEDGMENTS

The authors graciously acknowledge the Charles C. Chappelle Fellowship and the NASA Space Technology Research Fellowship for providing funding and support for this project.

REFERENCES

[1] Bidadi, S., Heister, S. D. and Matsutomi, Y. Computational and Experimental Study of Jet Interaction Fluidic Injectors. *Atomization and Sprays*, 21(2):127–138, Jan. 2011.

[2] Gregory, J. W., Sullivan, J. P., Raman, G. and Raghu, S. Characterization of the Microfluidic Oscillator. *AIAA Journal*, 45(3):568–576, Mar. 2007.

[3] Gregory, J. W., Sullivan, J. P. and Raghu, S. Visualization of jet mixing in a fluidic oscillator. *Journal of Visualization*, 8(2):169–176, Jan. 2005.

[4] Tomac, M. N. and Gregory, J. Frequency Studies and Scaling Effects of Jet Interaction in a Feedback-Free Fluidic Oscillator. *50th AIAA Aerospace Sciences Meeting including the New Horizons Forum and Aerospace Exposition*, pages 1–15, Jan. 2012.

[5] Tomac, M. N. Internal fluid dynamics and frequency characteristics of feedback-free fluidic oscillators. *Doctoral Dissertation, The Ohio State University*, pages 1–322, Jan. 2013.

[6] Khelfaoui, R., Colin, S., Orieux, S., Caen, R. and Baldas, L. Numerical and Experimental Analysis of Monostable Mini- and Micro-Oscillators. *Heat Transfer Engineering*, 30(1–2):121–129, Jan. 2009.

[7] Bobusch, B. C., Woszidlo, R., Bergada, J. M. Nayeri, C. N. and Paschereit, C. O. Experimental Study of the Internal Flow Structures Inside a Fluidic Oscillator. *Experiments in Fluids*, 54(6), June 2013.

[8] Cerretelli, C. and Gharaibah, E. An Experimental and Numerical Investigation on Fluidic Oscillators For Flow Control. *37th AIAA Fluid Dynamics Conference and Exhibit*, pages 1–9, June 2007.

[9] Shcherbik, D., Lubarsky, E., Neumeier, Y., Zinn, B. T., McManus, K., Fric, T. F. and Srinivasan, S. Suppression of Instabilities in Gaseous Fuel High-Pressure Combustor Using Non-Coherent Oscillatory Fuel Injection. *Proceedings of ASME Turbo Expo 2003 Power for Land, Sea, and Air*, pages 1–10, June 2003.

[10] Bennewitz, J. W., Lineberry, D. M. and Frederick, R. A. Investigation of a Single Injector with Applied High Frequency Pressure Disturbances For Applications To Liquid Rocket Engine Combustion Instabilities. *49th AIAA Joint Propulsion Conference*, pages 1–11, July 2013.

[11] Lubarsky, E., Shcherbik, D., Bibik, A. and Zinn, B. T. Active control of combustion oscillations by non-coherent fuel flow modulation. *9th AIAA Aeroacoustics Conference and Exhibit*, May 2003.

[12] Lubarsky, E., Shcherbik, D., Bibik, A. and Zinn, B. T. Open Loop Control of Severe Combustion Instabilities by Fuel Flow Modulation at Non Resonant Frequencies. *42nd AIAA Aerospace Sciences Meeting and Exhibit*, pages 1–19, Jan. 2004.

[13] Schadow, K., Gutmark, E. and Wilson, K. Active combustion control in a coaxial dump combustor. *26th AIAA/SAE/ASME/ASEE Joint Propulsion Conference*, pages 1–14, July 1990.

[14] Park, S., Ghosh, A., Diao, Q. and Yu, K. H. Optimizing Combustion Instability Suppression Using Secondary Fuel Injection. *47th AIAA/ASME/SAE/ASEE Joint Propulsion Conference & Exhibit*, pages 1–9, July 2011.

[15] Lee, J. G., Kim, K. and Santavicca, D. A. Effect of Injection Location on the Effectiveness of an Active Control System Using Secondary Fuel Injection. *Proceedings of the Combustion Institute*, 28:739–746, Jan. 2000.

[16] Altay, H. M., Speth, R. L., Hudgins, D. E. and Ghoniem, A. F. Flame-vortex interaction driven combustion dynamics in a backward-facing step combustor. *Combustion and Flame*, 156(5):1111–1125, May 2009.

[17] Guyot, D., Paschereit, C. O. and Raghu, S. Active Combustion Control Using a Fluidic Oscillator for Asymmetric Fuel Flow Modulation. *International Journal of Flow Control*, 1(2):155–166, July 2009.

[18] Tewes, P. and Taubert, L. Control of Separation on a Swept Wing using Fluidic Oscillators. *53rd AIAA Aerospace Sciences Meeting*, pages 1–15, Jan. 2015.

[19] Andino, M. Y., Lin, J. C., Washburn, A. E., Whalen, E. A., Graff, E. C. and Wygnanski, I. J. Flow Separation Control on a Full-Scale Vertical Tail Model using Sweeping Jet Actuators. *53rd AIAA Aerospace Sciences Meeting*, pages 1–14, Jan. 2015.

[20] Whalen, E. A., Lacy, D. S., Lin, J. C., Andino, M. Y., Washburn, A. E., Graff, E. C. and Wygnanski, I. J. Performance Enhancement of a Full-Scale Vertical Tail Model Equipped with Active Flow Control. *53rd AIAA Aerospace Sciences Meeting*, pages 1–11, Jan. 2015.

[21] Raman, G., Packiarajan, S., Papadopoulos, G., Weissman, C. and Raghu, S. Jet thrust vectoring using a miniature fluidic oscillator. *The Aeronautical Journal*, pages 129–138, Mar. 2005.

[22] Raman, G. and Raghu, S. Cavity resonance suppression using miniature fluidic oscillators. *AIAA Journal*, 42(12):2608–2611, Dec. 2004.

[23] Warren, R. W. Negative Feedback Oscillator. U.S. Patent, Nov. 1964.

[24] Raghu, S. Fluidic oscillators for flow control. *Experiments in Fluids*, 54(2), Feb. 2013.

[25] Gopalan, S., Russell, G. and Steerman, D. E. High efficiency, multiple throat fluidic oscillator. U.S. Patent, May 2012.

[26] Raghu, S. Feedback-free fluidic oscillator and method. U.S. Patent, July 2001.

[27] Denshchikov, A. V., Kondrat'ev, N. V and Romashov, A. N. Interaction between two opposed jets. *Fluid Dynamics*, Jan. 1978.

[28] Tomac, M. N. and Gregory, J. W. Internal jet interactions in a fluidic oscillator at low flow rate. *Experiments in Fluids*, 55(5), May 2014.

[29] Tomac, M. N. and Gregory, J. W. Internal Flow Physics of a Fluidic Oscillator in the Transition Regime. *Active Flow and Combustion Control*, pages 1–15, Oct. 2014.

[30] Gregory, J. W. Development of Fluidic Oscillators as Flow Control Actuators. *Doctoral Dissertation, Purdue University*, pages 102–2, July 2005.

[31] ANSYS® FLUENT® 14.5.7. *ANSYS, Inc*., 0.

[32] Meier, E. J. Investigation of Combustion Control in a Dump Combustor Using the Feedback Free Fluidic Oscillator. *Master's Thesis, Purdue University*, Aug. 2015.

[33] Wood, P., Hrymak, A., Yeo, R. and Johnson, D. Experimental and computational studies of the fluid mechanics in an opposed jet mixing head. *Phys. Fluids*, 3(5):1362–1368, May 1991.

[34] Li, W.-F., Huang, G.-F., Tu, G.-Y., Liu, H.-F. and Wang, F.-C. Experimental study of planar opposed jets with acoustic excitation. *Physics of Fluids*, 25(1):014108, Jan. 2013.

[35] Johnson, D. A., Wood, P. E. and Hrymak, A. N. The effect of geometrical parameters on the flow field of an opposed jet RIM mix head: equal flow and matched fluids. *The Canadian Journal of Chemical Engineering*, 74:40–48, Feb. 1996.